

# Profile-Based Face Recognition

I.A. Kakadiaris, H. Abdelmunim, W. Yang, and T. Theoharis  
Computational Biomedicine Lab, Depts. of Computer Science and Elec. & Comp.  
Engineering, Univ. of Houston, Houston, TX, USA  
<http://www.cbl.uh.edu/>\*

## Abstract

*In this paper, we introduce a new system for profile-based face recognition. The specific scenario involves a driver entering a gated area and using his/her side-view image (the driver remains seated in the vehicle) as identification. The system has two modes: enrollment and identification. In the enrollment mode, 3D face models of subjects are acquired and profiles extracted under different poses and stored to form a gallery database. In the identification mode, 2D images are acquired and the corresponding planar profiles are extracted and used as probes. Then, probes are matched to the gallery profiles to determine identity. The matching is accomplished using implicit shape registration via the vector distance functions. In our experiments, the approach using implicit registration exhibited higher accuracy than the iterative closest point methodology due to the use of more general transformations. The performance of our system is illustrated using a variety of databases.*

## 1. Introduction

Compared with other biometrics technologies, face recognition has garnered considerable attention in the last decades due to its non-intrusive characteristics. Numerous face recognition methods have been proposed [2, 20]. However, most of these methods are designed to work with frontal face images. In many cases, a frontal facial image is not available (e.g., the situation of a driver entering a gated area).

Profile-based face recognition poses several challenges: different poses, varying illumination, occlusion, and facial expressions. A system can use as input either the full side-view images or the silhouette of a subject's face.

This paper introduces a new approach for the

profile-based face recognition. The specific scenario involves a driver entering a gated area and using his/her side-view image (s/he sits inside the vehicle) as identification. The gallery includes face profile information under different poses collected from different subjects during enrollment. These profiles are generated by projecting the 3D face models. Probe profiles are extracted from the input images and compared with the gallery profiles. The comparison between different profiles is implemented using an implicit shape registration approach. Our contributions are: 1) employing 3D face models in the gallery database of the recognition system to handle rotation variations in the input probe images and hence improving the recognition rate; 2) using implicit registration for profile matching (which allows using general transformation functions, hence obtaining higher registration accuracy); and 3) designing a new system for recognizing drivers which can be applied at access control points.

The rest of this paper is organized as follows: A summary of the related research is presented in Sec. 2. Section 3 presents our methodology in detail. The experimental results and discussion are presented in Sec. 4, while conclusions and future work are provided in Sec. 5.

## 2. Previous Work

There exist two categories of approaches for side-view face recognition: appearance-based and profile-based methods. Appearance-based methods use the side-view face image as a direct input. Profile-based methods use the profile extracted from the side-view image.

In the appearance-based methods, there are two different scenarios for profile recognition. In the first, the probe is a side-view face image and the gallery is a frontal face image. This is an extreme situation of face recognition across pose. Detailed literature reviews about face recognition across pose are provided in [10, 21]. However, most methods are only able to

---

\*978-1-4244-2154-1/08/\$25.00 ©2008 IEEE

work on face images with limited variations in pose and the performance drastically decreases when applied to data with  $-90^\circ$  to  $90^\circ$  pose change. Blanz *et al.* [5] proposed face identification across different poses based on a 3D morphable model. However, the prealignment must be done manually and thus cannot achieve automatic recognition. In the second scenario, both the probe and gallery are side-view face images. This could be considered an example of multi-view face recognition [10, 21]. Pentland *et al.* [18] proposed to extend the popular eigenface approach on a database of 21 people with poses from  $-90^\circ$  to  $90^\circ$ . Zhou and Bhanu [23] proposed to apply PCA and multiple discriminant analysis for side-view face recognition. To align the side-view face images in both training and test datasets, the fiducial points extracted by a curvature-based method were used.

Generally, including the texture information of the human face results in more discriminating results. However, in an outdoor situation, the texture of the face is sensitive to illumination variations. The performance of appearance-based methods will deteriorate under changing lighting conditions. In contrast, profile-based methods use the shape information of the human face and are less sensitive to illumination changes. The method proposed in this paper falls under the profile-based recognition category.

Profile-based face recognition was first proposed in 1888 by Galton [8]. In the 1970's, Harmon *et al.* [12] published their seminal work in face profile recognition. They extracted the geometry features of the face profile to form a 10-dimensional feature vector according to the positions of 9 fiducial points on the profile. In their later work [11], the number of fiducial points was increased to 11 to form a 17-dimensional feature vector for each profile. A 96% recognition accuracy rate was reported.

Bhanu and Zhou [4] proposed a method using dynamic time warping (DTW) to match face profiles. According to the curvature value of each point on the profile, the pronasale and the nasion points are found and used to crop the face part and discard the non-face parts. The similarity score between the probe and each profile in the gallery are computed by the DTW based on curvature. Their method was evaluated on two side-view face databases, reporting a recognition rate of almost 90% as the best result. Zhou and Bhanu [22] extended this work to face profile recognition in video by constructing a high-resolution side face image from a series of aligned low-resolution side face images. Computing the fiducial point positions based on curvature in these methods is very crucial since it depends on scale-space preprocessing. This is

biased towards the size of the profile and the variance of the Gaussian applied to estimate the required scale. Applying the scale-space approach on different profiles does not guarantee the same curvature patterns in all cases. Liposcak *et al.* [14] proposed a scale-space filtering method based on fiducial-based features that exhibited a recognition rate of 90% when tested using data from 30 subjects.

Accurate localization of the fiducial points greatly affects the recognition results. To the best of our knowledge, there is no fiducial points detection algorithm which is able to work correctly and robustly on large databases. To overcome this, registration-based methods have been proposed.

Pan *et al.* [16] presented an experimental comparison for the face profile recognition problem. The authors compared different profile alignment methods, such as tangent-based normalization, 2D iterative closest point alignment (2D ICP) and simulated annealing (SA) alignment. In addition to the side-view face image databases, the profiles extracted from 3D database are also used to evaluate different methods. They concluded that the SA and 2D ICP method achieved the best recognition performance. Gao and Leung [9] proposed a string matching method for face profile recognition. The face profile is first transformed into a series of line segments. Then each line segment is represented by its attributes such as the length, orientation, and midpoint. After performing the merge domain string matching method, the distance score of the probe and the gallery profiles were computed. The approach assumes that the two compared profiles have the same curve details and fails whenever occlusion occurs. The two approaches described above use only 2D profiles (probe and gallery) ignoring the head pose variation which may occlude some part of the face profile. In their comparison, no results have been reported for the comparison between 2D and 3D profiles.

Wu *et al.* [19] proposed a face recognition method based on three different curves extracted from the 3D face model. Besides the face profile, they use two horizontal curves of a 3D face. After the registration between probe and gallery profiles using SA-based alignment, the partial Hausdorff score distance is applied to compute the similarity between the probe and gallery. This work addresses the problem only for 3D input data which is not the case in our target application. Recognizing 2D profiles is very important since obtaining the planar profiles from a digital image is much easier and widely applicable than extracting the three curves used in the above technique. Finally, in addition to human authentication, facial profile analysis has been applied in many areas (e.g., facial expression analysis [17], 3D



Figure 1. Hardware setup of the enrollment station.

face reconstruction [7]).

### 3. Methods

The main idea behind our approach is to compare 2D planar profiles against 3D face models and obtain the best match. The comparison is handled by projecting the 3D model for a given pose and obtaining the corresponding silhouette. These silhouettes represent profiles that can be registered and matched with the probes. This has many advantages. Storing 3D facial data allows greater flexibility, better understanding of face recognition issues, and requires no training compared to a statistical modeling approach. Projecting the 3D models to obtain 2D profiles simplifies the problem and avoids 2D/3D registration. Our face recognition system encompasses two modes, enrollment and identification.

**3.1 Enrollment:** Raw data are collected, and the metadata generated after processing are stored in our database: E.1) Data Acquisition, E.2) 3D Face Model Fitting, E.3) Generating a 2D Profile Gallery from the 3D Fitted Face Data.

**Step E.1: Data Acquisition:** The data acquisition hardware consists of a 2-pod 3dMD<sup>TM</sup> [1] system, a Canon DSLR, and a Logitech webcam. The system captures both a 2D face image and 3D face data simultaneously. The setup of data acquisition is depicted in Fig. 1. The 2-pod 3dMD<sup>TM</sup> system is used to acquire the 3D face data. The DSLR and webcam cameras capture different resolution images for the subject. Correspondences between the 3D data and the 2D images are established through calibration.

**Step E.2: Face Model Fitting:** This process aims to fit a generic face model to the 3D scan of the subject. Based on the work of Kakadiaris *et al.* [13], we use an annotated face model (AFM) that defines the control points of a subdivision surface and is annotated into different areas (e.g., mouth, nose, eyes). These facial areas have different properties associated

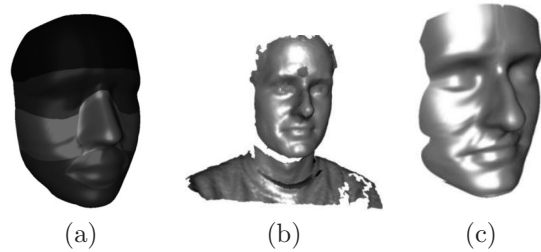


Figure 2. Depiction of: (a) AFM, (b) raw Data, and (c) fitted AFM.

with them which are used by our method. For example, the mouth area is considered less rigid than the nose area in the fitting step. Specifically, first, the model is globally aligned to the subject and local deformations are matched to the subject face area. An example is depicted in Fig. 2 where the generic face model is fitted to the subject scan to generate the corresponding fitted AFM. This step is necessary to obtain 3D face models suitable to form the gallery database (various examples are depicted in Fig. 3).

**Step E.3: Generating the Gallery Profiles:** The 3D face model is stored in the gallery database along with 2D planar profiles. For each pose, the model is projected using perspective projection given the corresponding camera parameters, resulting in a 2D binary image. The projection image is scanned line by line from left to right to keep the first white pixel (edge points) as a profile point, hence eliminating the non-profile parts. An example of a 3D face at four poses is depicted in Fig. 4. Using the AFM helps in marking different profile regions (e.g., nose, mouth) as depicted in Fig. 2(a). Detecting profile fiducial points can be performed automatically and stored in our gallery database.

**3.2 Identification:** This mode has the following steps: I.1) Data acquisition, I.2) Extracting probe profiles from input digital images, I.3) Registering the probe

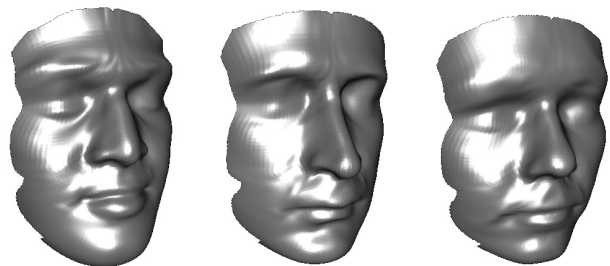


Figure 3. Selected fitted 3D face models from which gallery profiles are derived.

and gallery profiles, I.4) Computing the distance score and deciding the identity of the person by selecting the gallery profile with the minimum distance score to the probe.

**Step I.1: Data Acquisition:** The hardware at the identification station consists of a Canon DSLR and a Logitech webcam (Fig. 5). Using two different cameras allows different resolutions for the same subject and hence we can explore the effect of resolution on the recognition results.

**Step I.2: Profile Extraction from Side-View Face Image:** The face detection software developed by Pittsburgh Pattern Recognition, Inc. is applied to the side-view facial image to detect the facial area. The profile extraction process is currently performed by the semi-automatic approach of live-wire as described by Chodorowski *et al* [6]. By marking an initial position

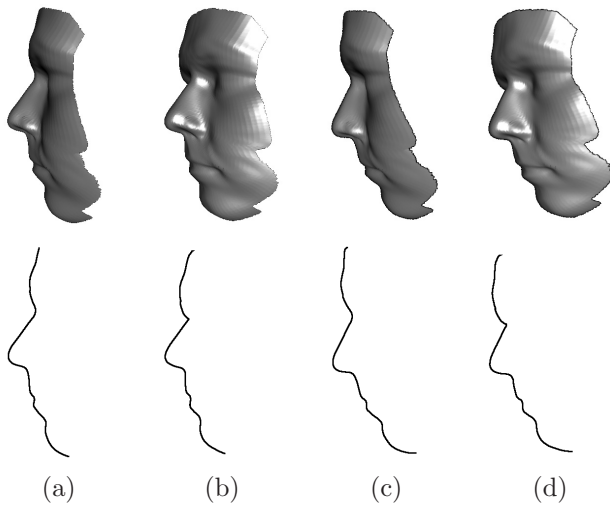


Figure 4. The top row illustrates a 3D face model at different poses. The bottom row depicts the corresponding gallery profiles: (a) standard pose profile, (b) rotation around x-axis only by  $10^\circ$ , (c) rotation around y-axis only by  $10^\circ$ , and (d) rotation around x-axis followed by rotation around y-axis ( $10^\circ$  for each). Note that the z-axis points outwards from the face.



Figure 5. Hardware setup of the Identification station.

and then moving along the face profile, we can extract the profile curve. An example of a side-view image and its profile are depicted in Fig. 6.

**Step I.3: Profile Registration:** Determining point-wise correspondences (between two given 2D shape profiles  $\alpha$  and  $\beta$ ) is the objective of the profile registration. The first profile is called the source (or moving) shape while the other is called the target. A transformation  $\mathbf{A} = \mathbf{A}(\mathbf{X})$  that includes scale  $\mathbf{S}$ , rotation  $\mathbf{R}$ , and translation  $\mathbf{T}$ , is considered. This paper uses an implicit registration approach. However, for the sake of comparison, we will start by illustrating a modified version of the iterative closest point (ICP) algorithm.

**ICP Registration:** Iterative Closest Point (ICP) [3], has been applied widely to the 3D shape registration problem. Good initialization is required for the ICP to converge as fast as possible and provide good registration. Each profile has two end points (upper point  $A$  and lower point  $B$ ) and the nose tip ( $C$ ). The nose tip is marked automatically as the point with the maximum distance from the line passing through the end points (measured in the normal direction). Estimating the initial parameters is performed as follows:

1. **Scaling:** According to the Euclidean distance between the two points  $B$  and  $C$ , a uniform scale factor is computed.
2. **Rotation:** The source profile is rotated so as to make the slope of the line defined by  $C$  and  $B$  match the slope of the equivalent line in the target profile.
3. **Translation:** The source profile is translated to make the point  $C$  on both profiles match.

After the coarse alignment, the conventional ICP algorithm is used to enhance the registration results.

**Implicit Registration:** For implicit registration, the vector distance function (VDF) representation [15] is used. This kind of registration does not need any

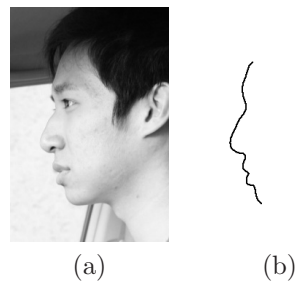


Figure 6. Face profile extraction: (a) a side-view face image and (b) its profile curve.

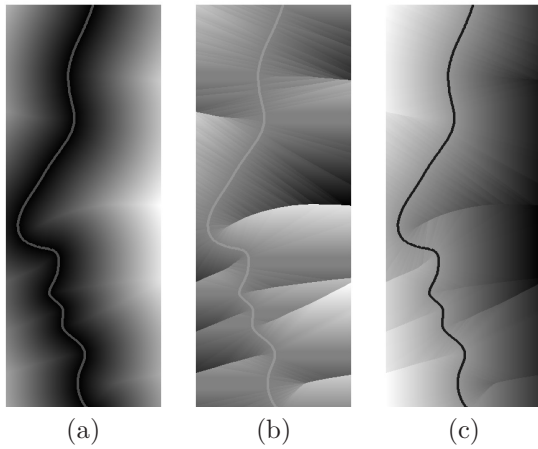


Figure 7. Shape representation (gray level map): (a) conventional distance transformation function, (b) the first projection of the vector function ( $\phi_1$ ), (c) the second projection of the vector function ( $\phi_2$ ).

point correspondences. The profile is defined implicitly by the function  $\Phi : R^2 \rightarrow R^2$ . This function represents the vector from the current point to the closest position on the profile. An example is given for one of the database profiles in Fig. 7 with the conventional distance transform. The profile points always satisfy the condition  $|\Phi| = 0$ . The function has two components (projections) defined as  $\phi_1$  and  $\phi_2$ . A vector dissimilarity measure can be computed directly as:  $\mathbf{r} = \Phi_\beta(\mathbf{A}) - \mathbf{S}\mathbf{R}\Phi_\alpha(\mathbf{X})$ , where  $\Phi_\alpha$  and  $\Phi_\beta$  represent the VDF representations of profiles  $\alpha$  and  $\beta$ . Scaling, rotating, and translating the profile results in a new map that can be computed directly from the original one. This kind of representation is more suitable for the profile shape (open curve) than the usual conventional distance map. Thus, the energy to be minimized will be the sum of the squared dissimilarity measures as follows:

$$E(\mathbf{S}, \mathbf{R}, \mathbf{T}) = \int_{\Omega} \mathbf{r}^T \mathbf{r} d\Omega.$$

The complexity of the problem is reduced by considering only points around the zero level of the vector function since distant points can be neglected using the narrow band selection function  $\delta$  [15]. The matching space is limited to a small band around the curve that can be selected by introducing the following energy function:

$$E(\mathbf{S}, \mathbf{R}, \mathbf{T}) = \int_{\Omega} \delta_{\epsilon}(\Phi_{\alpha}, \Phi_{\beta}) \mathbf{r}^T \mathbf{r} d\Omega.$$

Note that the scale in this case is more general than that used with the ICP method and hence we obtain

better registration. The optimization of this function is accomplished using a gradient descent approach.

**Step I.4: Computing Distance Between Different Profiles:** Next, we define a distance score between two registered profiles. Let  $\mathbf{C}(p) : [0, 1] \in R \rightarrow R^2$  be a planar profile curve with a parameter  $p$ . We use the 2-norm distance definition to compare the profiles after the registration step as follows:

$$\xi = \int_{p=0}^1 \|\mathbf{C}^{\alpha}(p) - \mathbf{C}^{\beta}(q)\| dp,$$

where  $\mathbf{C}^{\beta}(q)$  is the closest point on the profile  $\beta$  to the point  $\mathbf{C}^{\alpha}(p)$  on profile  $\alpha$ . Using an implicit representation for the profiles, the score can be written as follows:

$$\xi' = \int_{\Omega} \delta_{\epsilon}(\Phi_{\alpha}) \|\Phi_{\alpha} - \Phi_{\beta}\| d\Omega.$$

where  $\delta$  is defined only around the zero crossing of  $\Phi_{\alpha}$  and  $\epsilon \rightarrow 0$ .

## 4. Experimental Results

For our experiments, we created four different databases with different conditions as follows:

**D<sub>1</sub>:** consists of 40 side face images from 10 subjects (Fig. 8). Image resolution is  $1280 \times 1024$ . The images were acquired in a standard profile view. Five subjects wear glasses.

**D<sub>2</sub>:** contains 69 side face images from 10 subjects. Subjects are asked to assume standard pose and remove their glasses. Image resolution is  $3888 \times 2592$ .

**D<sub>3</sub>:** consists of 96 side face images from 9 subjects. The subjects are asked to assume a variety of poses. The images have the same resolution as the images in **D<sub>2</sub>**. The above three databases contain side-view images under different conditions from the same subjects. **D<sub>4</sub>:** contains 289 side face images from 44 subjects. Each subject is asked to assume 5 to 6 poses without glasses. Its images have the same resolution as the images in **D<sub>2</sub>**.

3D face data have been captured for eleven subjects. Their 3D face models are generated by fitting the AFM. Each 3D model is projected at different poses to generate its gallery profile. Four poses are considered which result in 44 gallery profiles. Two different techniques are considered for the registration process: ICP and implicit registration using VDF. The Cumulative Match Characteristic (CMC) and the Receiver Operating Characteristic (ROC) curves are plotted in each case. We notice that recognition rate is enhanced (by using VDF registration) in **D<sub>1</sub>** by about 10% and **D<sub>3</sub>** by almost 2% (Fig. 9). The ICP-based approach results in a better performance in **D<sub>2</sub>** by about 1.5%.



Figure 8. Sample images from the four databases ( $D_1$ ,  $D_2$ ,  $D_3$ , and  $D_4$ ) given in each row.

The improvement using the implicit registration is expected since the technique allows using a more general transformation and hence achieves better registration. However, that did not occur with the data from  $D_2$  because sometimes a profile is perfectly registered with another profile of a different subject. This results in a mismatch when the score considers only the distance between the profiles. Another advantage of using the implicit registration technique is that it does not need any point correspondences. The results obtained using  $D_1$  are recorded for the implicit registration using only one pose gallery which implies that the registration is more successful than ICP (which uses 4 poses). Recognition rate for the profiles of  $D_3$  is low for both methods since the profiles in this case have larger pose variations than those considered with the gallery. In addition, this database contains datasets with different facial expressions.

The ROC depicts the advantage of using implicit registration over ICP (Figs. 10(a-c)). The equal error rate (EER) shows the difference between the two registration techniques results in Fig. 10. There is a large difference in  $D_2$  ROC results which means that ICP does not deliver perfect registration even with the same subject profiles. In Fig. 10(d), we observe that using four poses (corresponding to different rotations of the 3D model) in the gallery database enhances the performance of the system. The ROC is improved especially at low false acceptance rates.

For tests using  $D_4$ , we created a gallery with 3 poses for each of the 44 subjects. Again, identification results have been measured and the CMC curve is plotted in

Fig. 11(a). At rank 1, the implicit registration still yields better results by about 4%. The ICP approach results in missing 12 probes more than VDF in identification. Also, it is clear that using multi-pose projections in the gallery enhanced the results by 6.43% (Fig. 11). Using additional poses will enhance the results but will affect the computational time dramatically.

## 5. Conclusion

We have presented a profile-based recognition system. We illustrated the set-up for the approach to be used for recognition of car drivers from their side-view images. Profile distance measures are computed after minimizing the difference between the probe and gallery using two different registration techniques. Four different databases are used to provide probe profiles. The 3D face models are used to generate gallery profiles. The 3D model is projected at different poses to overcome the profile changes in the probe images due to head pose. Implicit registration shows better performance than that of the ICP.

**Acknowledgments:** Finally, we would like to thank our sponsors. This work was funded in part by the Central Intelligence Agency under the DISA ENCORE contract DCA200-02-D-5014 with Unisys Corporation serving as the prime on behalf of the Government. Any opinions, findings, conclusions or recommendations expressed in this material are of the authors' and may not reflect the views of the sponsors.

## References

- [1] 3dMD. <http://www.3dmd.com/>.

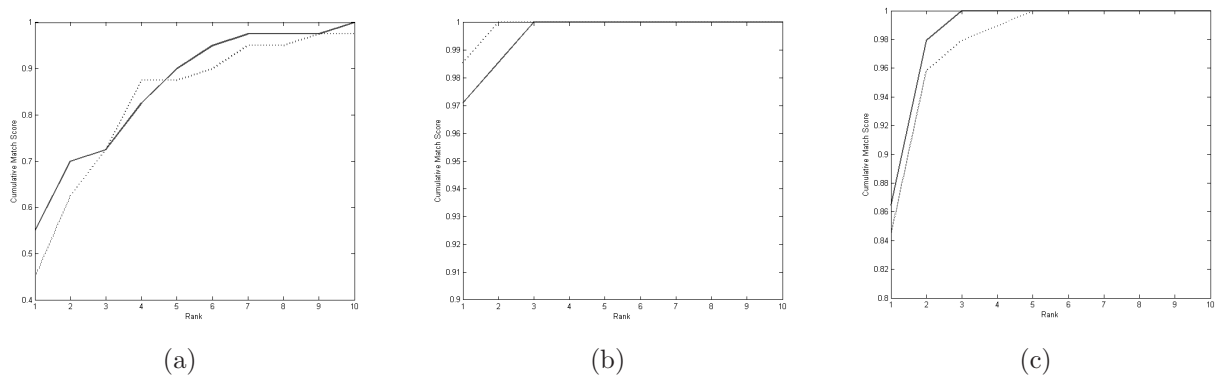


Figure 9. CMC curves for (a)  $D_1$ , (b)  $D_2$ , and (c)  $D_3$ . The dotted line indicates the results obtained using the ICP registration, while the solid line represents the results obtained using the VDF approach.

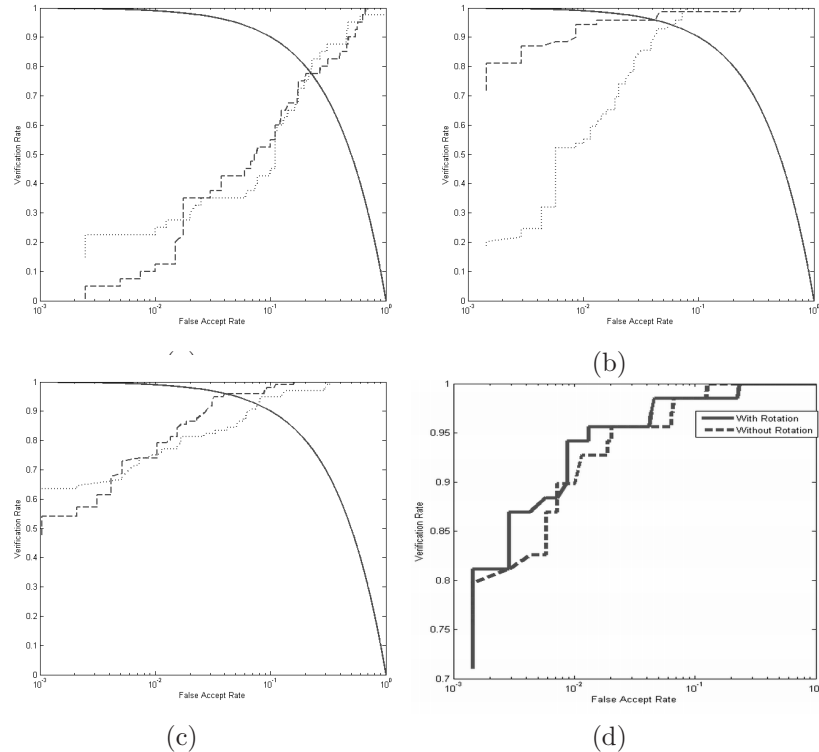


Figure 10. ROC curves for (a)  $D_1$ , (b)  $D_2$ , and (c)  $D_3$ . The dotted line indicates the results obtained using the ICP registration, while the dashed line represents the results obtained using the VDF approach. The equal error rate curve is represented by the solid line. The difference between using a gallery with only a standard pose (no rotation) projection and another which has different poses (with rotations) is illustrated in (d).

- [2] P. Belhumeur, J. Hespanha, and D. Kriegman. Eigenfaces vs. fisherfaces: recognition using class specific linear projection. *IEEE Transactions on Pattern Analysis and Machine Intelligence*, 19(7):711–720, 1997.
- [3] P. J. Besl and N. D. McKay. “A method for registration of 3-D shapes”. *IEEE Transactions on Pattern Analysis and Machine Intelligence*, 14:239–256, 1992.
- [4] B. Bhanu and X. Zhou. Face recognition from face profile using dynamic time warping. In *Proc. International Conference on Pattern Recognition*, pages IV: 499–502, Cambridge, England, UK, 2004.
- [5] V. Blanz, S. Romdhani, and T. Vetter. Face identification across different poses and illuminations with a 3D morphable model. In *Proc. IEEE International Conference on Automatic Face and Gesture Recognition*, pages 192–197, Washington, DC, USA, 2002.
- [6] A. Chodorowski, U. Mattsson, M. Langille, and G. Hamarneh. Color lesion boundary detection using

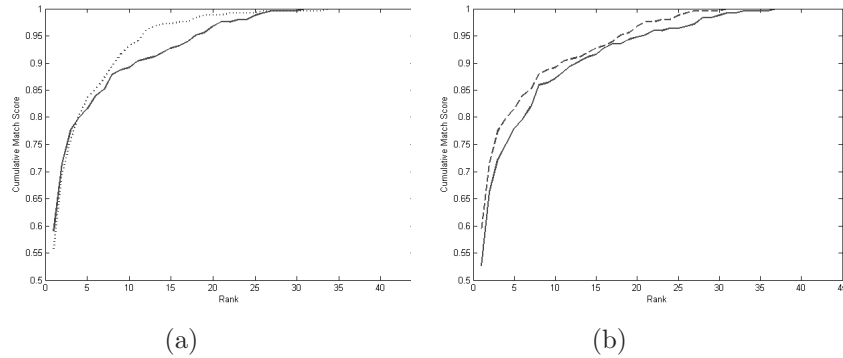


Figure 11. CMC results for the database  $D_4$ : (a) The dotted line indicates the results obtained using the ICP registration, while the dashed line represents the results obtained using the VDF approach. (b) Results using a gallery with a standard pose are illustrated by the dashed line while the effect of using different poses is illustrated by the solid line (in both cases the VDF registration is used).

- live wire. In *Proc. SPIE Medical Imaging: Image Processing*, volume 5747, pages 1589–1596, Bellingham, WA, 2005.
- [7] B. Dariush, S. Kang, and K. Waters. Spatiotemporal analysis of face profiles: Detection, segmentation, and registration. In *Proc. IEEE International Conference on Automatic Face and Gesture Recognition*, pages 248–253, Nara, Japan, 1998.
- [8] F. Galton. Personal identification and description. *Nature*, 38:173–177, June 1888.
- [9] Y. Gao and M. Leung. Human face profile recognition using attributed string. *Pattern Recognition*, 35(2):353–360, February 2002.
- [10] R. Gross, S. Baker, I. Matthews, and T. Kanade. Face recognition across pose and illumination. In S. Z. Li and A. K. Jain, editors, *Handbook of Face Recognition*. Springer-Verlag, June 2004.
- [11] L. Harmon, M. Kaun, R. Lasch, and P. Ramig. Machine identification of human faces. *Pattern Recognition*, 13(2):97–110, 1981.
- [12] L. Harmon, S. Kuo, P. Ramig, and U. Raudkivi. Identification of human face profiles by computer. *Pattern Recognition*, 10(5-6):301–312, 1978.
- [13] I. Kakadiaris, G. Passalis, G. Toderici, Y. Lu, N. Karambatziakis, N. Murtuza, and T. Theoharis. 3D face recognition in the presence of facial expressions: An annotated deformable model approach. *IEEE Transactions on Pattern Analysis and Machine Intelligence*, 29(4):640–649, Apr. 2007.
- [14] Z. Liposcak and S. Loncaric. A scale-space approach to face recognition from profiles. In F. Solina and A. Leonardis, editors, *Proc. 8th International Conference on Computer Analysis of Images and Patterns*, volume 1689, pages 243–250, Ljubljana, Slovenia, September 1-3 1999. Springer.
- [15] H. A. E. Munim and A. Farag. Shape representation and registration using vector distance functions. In *Proc. IEEE Computer Society Conference on Computer Vision and Pattern Recognition*, pages 1–8, Minneapolis, Minnesota, USA, 2007.
- [16] G. Pan, L. Zheng, and Z. Wu. Robust metric and alignment for profile-based face recognition: An experimental comparison. In *Proc. 7th IEEE Workshop on Applications of Computer Vision*, pages I: 117–122, Breckenridge, CO, USA, 2005.
- [17] M. Pantic and I. Patras. Dynamics of facial expression: Recognition of facial actions and their temporal segments from face profile image sequences. *IEEE Transactions on Systems, Man and Cybernetics*, 36(2):433–449, April 2006.
- [18] A. Pentland, B. Moghaddam, and T. Starner. View-based and modular eigenspaces for face recognition. In *Proc. IEEE Computer Society Conference on Computer Vision and Pattern Recognition*, pages 84–91, Seattle, WA, USA, 1994.
- [19] Y. Wu, G. Pan, and Z. Wu. Face authentication based on multiple profiles extracted from range data. In *Proc. 4th International Conference on Audio- and Video-Based Biometric Person Authentication*, pages 515–522, Rye Town, NY, USA, 2003.
- [20] W. Zhao, R. Chellappa, P. Phillips, and A. Rosenfeld. “Face recognition: A literature survey”. *ACM Computing Surveys*, pages 399–458, 2003.
- [21] W. Zhao, R. Chellappa, P. Phillips, and A. Rosenfeld. Face recognition: A literature survey. *Computing Surveys*, 35(4):399–458, December 2003.
- [22] X. Zhou and B. Bhanu. Human recognition based on face profiles in video. In *Proc. IEEE Computer Society Conference on Computer Vision and Pattern Recognition*, pages III: 15–15, San Diego, CA, USA, 2005.
- [23] X. Zhou and B. Bhanu. Integrating face and gait for human recognition at a distance in video. *IEEE Transactions on Systems, Man and Cybernetics*, 37(5):1119–1137, October 2007.